NUMERICAL SIMULATION OF THE SETTLING OF POLYDISPERSE SUSPENSIONS OF SPHERES

R. BÜRGER[a,*], F. CONCHA[b], K. K. FJELDE[c,d], AND K. HVISTENDAHL KARLSEN[c,d]

Abstract. The extension of Kynch's kinematical theory of ideal suspensions to polydisperse suspensions of spheres leads to a nonlinear system of conservation laws for the volumetric concentration of each species. In this work, we consider particle species different in sizes and densities, including the buoyant case. We show that modern shock-capturing numerical schemes for the solution of systems of conservation laws can be employed as an efficient tool for the simulation of the settling and separation of polydisperse suspensions. This is demonstrated by comparison with published experimental and theoretical results and by simulating some hypothetical configurations. Particular attention is focused on the emergence of rarefaction waves.

1. Introduction

The one-dimensional sedimentation of ideal suspensions of monosized spheres under the influence of gravity can be described quite well by Kynch's sedimentation theory [1, 2, 3]. The principal assumption of this theory is that the local settling velocity, or solids phase velocity, is a function only of the local volumetric solids concentration. For the settling of a suspension of homogeneous initial concentration ϕ_0 in a column of height L, this theory leads to an initial value problem of a hyperbolic conservation law of the type

$$(1)\qquad \begin{gathered} \frac{\partial \phi}{\partial t} + \frac{\partial}{\partial z}\big(\phi v_{\mathrm{s}}(\phi)\big) = 0, \quad 0 \leq z \leq L, \quad t > 0; \\ \phi(z,0) = \phi_0(z) = \begin{cases} 0 & \text{for } z > L, \\ \phi_0 & \text{for } 0 \leq z \leq L, \\ \phi_{\max} & \text{for } z < 0, \end{cases} \end{gathered}$$

Key words and phrases. Polydisperse suspensions; kinematical sedimentation process; kinematic shocks; rarefaction waves; slip velocities; shock-capturing schemes.

[a]Institute of Mathematics A, University of Stuttgart, Pfaffenwaldring 57, D-70569 Stuttgart, Germany, e-mail: `buerger@mathematik.uni-stuttgart.de`.

[b]Department of Metallurgical Engineering, University of Concepción, Casilla 53-C, Concepción, Chile, e-mail: `fconcha@udec.cl`.

[c]Department of Mathematics, University of Bergen, Johs. Brunsgt. 12, N-5008 Bergen, Norway, e-mail: `kennethk@mi.uib.no`.

[d]RF-Rogaland Research, Thormølensgt. 55, N-5008 Bergen, Norway, e-mail: `Kjell-Kaare.Fjelde@rf.no`.

*Corresponding author.

where $\phi_0 \in [0, \phi_{\max}]$; $\phi_{\max} \in (0,1]$ is the maximum concentration and v_{s} is the solids phase velocity. A constitutive equation for the Kynch batch flux density function $f(\phi) := \phi v_{\mathrm{s}}(\phi)$ must be postulated. This function is assumed to satisfy

$$f(\phi) < 0 \ \text{ for } \phi \in (0, \phi_{\max}), \quad f(0) = f(\phi_{\max}) = 0, \quad f'(0) < 0 \ \text{ and } f'(\phi_{\max}) > 0. \tag{2}$$

To motivate this study of the settling of polydisperse suspensions, we briefly review some known results for monodisperse suspensions. It is well known that solutions of hyperbolic conservation laws with such flux density functions develop discontinuities after finite time, even if the initial data are smooth. This in turn requires a selection principle, or entropy condition, to determine the physically relevant solution, called entropy weak solution, from possibly several weak solutions. Bustos and Concha [4] consider flux density functions f with at most two inflection points; this assumption covers the vast majority of empirical flux density functions encountered in practice. Using the method of characteristics, they determine exact entropy weak solutions to problem (1), for some cases of ϕ_0 and $f(\phi)$. The complete solution of problem (1) for flux density functions with at most two inflection points consists of seven qualitatively different modes of sedimentation, depending on the value of ϕ_0 and on $f(\phi)$, and is presented by Bustos *et al.* in [5].

Kynch's theory has also been applied to continuous sedimentation, where a convective term is added to the flux density function [6]–[10] and it has been reformulated as part of a general phenomenological theory of sedimentation. This theory, which has recently been extended to a multidimensional framework [11], includes sedimentation models for flocculated suspensions which lead to a parabolic-hyperbolic degenerating equation instead of the hyperbolic conservation law given in (1), see [12, 13].

While the settling of ideal and flocculated suspensions of monosized particles has been studied extensively, the implications of the mathematical models proposed for the settling of polydisperse suspensions, containing two or more particle species differing in size or density, are not yet well understood. In particular, a complete analytical solution of batch settling processes for initially homogeneous polydisperse suspensions as an analogue of Bustos and Concha's classification [4] is not available.

Several authors have formulated constitutive equations for such polydisperse suspensions. Smith [14, 15] was one of the first who proposed a mathematical model for the sedimentation of polydisperse suspensions with particles of different sizes. However, the agreement between the model predictions and his own experimental data remained unsatisfactory. Lockett and Al-Habbooby studied the settling of polydisperse suspensions of particles of different sizes [16] as well as of different densities [17] and assumed that the velocity relative to the fluid, or slip velocity, of each species was a function only of the total volumetric solids concentration. The motion of nearby particles was not taken into account, leading to an overestimation (in absolute value) of the settling velocities. Mirza and Richardson [18] extended the Lockett and Al-Habbooby model to polydisperse suspensions and introduced a correction factor, again depending on the total local solids volume fraction, to improve accordance between model predictions and experimental results. Masliyah [19] considered the drag force exerted on each particle species and obtained a more general expression of the slip velocity for each species, which will be employed in this paper. This expression contains the hindered settling function known from the theory of sedimentation of monodisperse suspensions, which is now applied to the total solids volume fraction (the sum of the volume fractions of all species) or, equivalently, to the fluid volume fraction or porosity. Patwardhan and Tien [20] propose improving the accuracy of Masliyah's expression by replacing the porosity by a new quantity, the apparent porosity. Law *et al.* [21] compare the predictions of these models, in combination with several approaches for the hindered settling function, with experimental results for the separation of a suspension of heavy and light (buoyant) particles.

Concha *et al.* [22] recognize that Masliyah's equations [19] for the slip velocity of each species can be viewed as an extension of Kynch's theory to polydisperse suspensions, since now the solid-fluid relative velocity for each species is assumed to be given as a function of the local solids species volume fractions only. Similar to the previous authors, they obtain a system of N conservation laws for the local volumetric concentrations $\phi_1, \dots, \phi_N$, each representing different particle species. It should be noted, however, that only few other researchers, e.g., Shih *et al.* [23], have actually embedded these equations into the mathematical terminology of conservation laws.

As mentioned before (see also [24]), conservation laws produce discontinuous solutions. In the context of sedimentation, these discontinuities in the solids concentrations are also referred to as kinematic shocks [25, 26]. Their propagation velocities are given by the Rankine-Hugoniot condition in terms of the adjacent concentration values. In addition, a shock must satisfy a certain admissibility criterion or entropy condition.

Several authors, including Greenspan and Ungarish [27], Mirza and Richardson [18], Selim *et al.* [28] and Stamatakis and Tien [29] propose solution procedures for the problem of settling of initially homogeneous polydisperse suspensions in a column based on explicitly tracking kinematic shocks between areas of presumed constant concentrations. This is in accordance with the widely observed batch settling behaviour of a suspension of K particle species: an initially homogeneous suspension will develop K upper discontinuities, separating $K+1$ zones in which the concentrations are constant.

The first zone (counted from above to below) would contain only clear liquid, the second only liquid and the particle species of smallest (in modulus) final settling velocity; the third liquid and solid particles with the smallest and with the second smallest final velocities, and so on, until a zone is reached in which all solids species are present at their initial concentration. At the same time, one discontinuity emerges from the bottom of the vessel below which the total solids volume fraction is assumed to attain its maximum value. This rising discontinuity will intersect at some time the fastest discontinuity traveling downwards, yielding a change of propagation velocity of the rising sediment level and a change of the sediment composition. This solution procedure will be briefly outlined in mathematical terms later. However, to our view, the major shortcoming of this construction is its inability to describe continuous transitions described by rarefaction waves.

It is the purpose of the present work to extend the study by Concha *et al.* [22], by admitting that the species may have different sizes and densities, by including a modified flux density function, by utilizing an improved boundary condition and by considering non-homogeneous initial data. Moreover, we show that modern shock-capturing numerical schemes for the solution of nonlinear systems of conservation laws can be employed successfully to simulate sedimentation processes, and that they reproduce rarefaction waves occurring during the formation of the sediment. This is demonstrated by numerical simulation of published experimental, theoretical and numerical results and three hypothetical configurations. In addition, we get an insight into the possible structure of the exact solutions to the problems solved.

The solution of these equations by analytical techniques, in particular, of the Riemann problem consisting of two different adjacing constant states, still seems difficult, therefore numerical schemes should be employed. In a separate paper with emphasis on numerical analysis [30], we compare the performance of various numerical schemes when applied to the system of equations developed in this paper. The common features of these schemes is that they detect and reproduce discontinuities automatically and only where they are admissible, which makes explicit shock tracking unnecessary. The numerical examples presented here are high-accuracy calculations obtained by the shock-capturing scheme introduced by Nessyahu and Tadmor [31].

2. Kinematical sedimentation model for polydisperse suspensions

Consider an ideal suspension of a fluid with spherical particles of N different diameters d_i, $i = 1, \dots, N$ and M different densities ϱ_j, $j = 1, \dots, M$. We denote by v_{f} the local velocity of the fluid and by v_{ij} and $\phi_{ij} = \phi_{ij}(z,t)$ the phase velocity and the volumetric concentration, respectively, of particles of diameter d_i and density ϱ_j. The mass balances for the solids can then be written as

$$\frac{\partial \phi_{ij}}{\partial t} + \frac{\partial}{\partial z} f_{ij} = 0, \quad i = 1, \dots, N, \quad j = 1, \dots, M, \tag{3}$$

where $f_{ij} = \phi_{ij} v_{ij}$. Taking into account kinematical constraints and constitutive assumptions, we now show that f_{ij} actually depends on all $M \cdot N$ volumetric concentrations ϕ_{ij}. For batch sedimentation, the volume average velocity

$$q := (1-\phi) v_{\mathrm{f}} + \sum_{i=1}^{N} \sum_{j=1}^{M} \phi_{ij} v_{ij} \tag{4}$$

vanishes, where

$$\phi := \sum_{i=1}^{N} \sum_{j=1}^{M} \phi_{ij}$$

denotes the solids total volume fraction: this can be checked by summing equations (3) over $i = 1, \dots N$ and $j = 1, \dots, M$ and the continuity equation of the fluid,

$$\frac{\partial}{\partial t}(1-\phi) + \frac{\partial}{\partial z}\left((1-\phi) v_{\mathrm{f}}\right) = 0, \tag{5}$$

which yields $\partial q / \partial z = 0$, and noting that $q = 0$ at $z = 0$. In terms of the solid-fluid relative velocities or slip velocities defined by $r_{ij} := v_{ij} - v_{\mathrm{f}}$ for $i = 1, \dots, N$ and $j = 1, \dots, M$, equation (4) can also be written as

$$v_{\mathrm{f}} = -\sum_{i=1}^{N}\sum_{j=1}^{M} \phi_{ij} r_{ij}. \tag{6}$$

Using (6) in

$$f_{ij} = \phi_{ij} v_{ij} = \phi_{ij}\left(r_{ij} + v_{\mathrm{f}}\right), \quad i = 1, \dots, N, \quad j = 1, \dots, M,$$

and defining the matrix of concentration values

$$\mathbf{\Phi} := \left(\phi_{ij}\right)_{i=1,\dots,N,\, j=1,\dots,M},$$

we obtain

$$f_{ij} = f_{ij}(\mathbf{\Phi}) = \phi_{ij}\Big(r_{ij} - \sum_{h=1}^{N}\sum_{k=1}^{M} \phi_{hk} r_{hk}\Big), \quad i = 1, \dots, N, \quad j = 1, \dots, M. \tag{7}$$

Next, constitutive equations for the relative velocities r_{ij} are postulated. Following Masliyah [19], Concha *et al.* [22] suggest, in the case of a constant and unique solids particle density ϱ_{s} (which makes a second index unnecessary), setting

$$r_i = r_{\infty i} V(\phi), \quad i = 1, \dots, N \tag{8}$$

and using the common formula

$$V(\phi) = V^{\mathrm{RZ}}(\phi) := (1-\phi)^n, \quad n > 1, \quad 0 \le \phi \le \phi_{\mathrm{max}} \tag{9}$$

as an extension of Richardson and Zaki's well-known formula [32] to the polydisperse case, where

$$r_{\infty i} = -\frac{1}{18}\frac{(\varrho_{\mathrm{s}} - \varrho_{\mathrm{f}}) g d_i^2}{\mu_{\mathrm{f}}}, \quad i = 1, \dots, N \tag{10}$$

is the Stokes settling velocity of a single particle of diameter d_i in a quiescent fluid of density ϱ_{f} and dynamic viscosity μ_{f}. The function $V(\phi)$ is frequently referred to as drag law [27] or hindered settling function [33]. Equation (8) can be extended to the suspensions considered here in a natural way; we set

$$r_{ij} = r_{\infty ij} V(\phi), \quad i = 1, \dots, N, \quad j = 1, \dots, M$$

and define the local density of the mixture

$$\varrho(\mathbf{\Phi}) = (1-\phi)\varrho_{\mathrm{f}} + \sum_{i=1}^{N}\sum_{j=1}^{M} \phi_{ij}\varrho_j,$$

which is the density of the fluid in which a single sphere is now assumed to settle. Instead of (10), we obtain

$$r_{\infty ij} = -\frac{1}{18}\frac{(\varrho_j - \varrho(\mathbf{\Phi})) g d_i^2}{\mu_{\mathrm{f}}}, \quad i = 1, \dots, N, \quad j = 1, \dots, M. \tag{11}$$

A rigorous derivation of this formula, considering the steady state momentum equations of each particle species, has been provided by Masliyah [19] following Wallis [34, Ch. 3]. Defining the parameters

$$\mu = -\frac{gd_1^2}{18\mu_{\mathrm{f}}}, \quad \delta_i = \frac{d_i^2}{d_1^2}, \quad i = 1, \ldots, N,$$

this leads to

$$f_{ij}(\mathbf{\Phi}) = \mu V(\phi)\phi_{ij}\Big(\delta_i\big(\varrho_j - \varrho(\mathbf{\Phi})\big) - \sum_{h=1}^{N}\delta_h \sum_{k=1}^{M}\phi_{hk}\big(\varrho_k - \varrho(\mathbf{\Phi})\big)\Big), \quad i = 1, \ldots, N, \quad j = 1, \ldots, M. \tag{12}$$

Writing $\mathbf{f}(\mathbf{\Phi}) := (f_{11}(\mathbf{\Phi}), f_{12}(\mathbf{\Phi}) \ldots, f_{1M}(\mathbf{\Phi}), f_{21}(\mathbf{\Phi}), \ldots, f_{NM}(\mathbf{\Phi}))^{\mathrm{T}}$, we obtain the system of $M \cdot N$ equations for the same number of unknowns

$$\frac{\partial \mathbf{\Phi}}{\partial t} + \frac{\partial \mathbf{f}(\mathbf{\Phi})}{\partial z} = 0, \quad 0 \le z \le L, \quad t > 0. \tag{13}$$

We assume that an initial concentration distribution

$$\mathbf{\Phi}(z, 0) = \mathbf{\Phi}^0(z), \quad 0 \le z \le L, \quad 0 \le \sum_{i=1}^{N}\sum_{j=1}^{M}\phi_{ij}^0(z) \le \phi_{\max} \tag{14}$$

is given, and that the boundary conditions are given by the zero flux conditions

$$\mathbf{f}|_{z=0} = 0, \quad \mathbf{f}|_{z=L} = 0, \quad t > 0. \tag{15}$$

Since there is no mass transfer between the spheres and the liquid and since both are incompressible, the total mass of particle species ij remains constant during the settling process. This means that only those equations

$$\frac{\partial \phi_{ij}}{\partial t} + \frac{\partial f_{ij}(\mathbf{\Phi})}{\partial z} = 0, \quad 0 \le z \le L, \quad t > 0$$

of the system (13) have to be solved for which $\phi_{ij}^0(z) \not\equiv 0$. For configurations in which the number of particle species not having density and size with others in common is relatively large and hence the number of equations actually to be solved is small compared to $M \cdot N$, a vector notation of the concentrations, omitting one index, is certainly more convenient.

In the monodisperse case ($N = M = 1$), equation (8) implies that concentration values ϕ near to one propagate at arbitrarily slow speed since $f'(1) = 0$, and that a batch sedimentation process never terminates. Concha *et al.* [22] overcome this shortcoming by requiring that the cumulative concentration ϕ at the bottom of a settling column attains immediately its maximum value $\phi_{\max}$, corresponding to the instantaneous formation of a packed bed when sedimentation starts. However, it is not evident how to determine the required N boundary concentrations from this value. It is more natural to require that all flux densities vanish at $z = 0$ as expressed in (15), in combination with utilizing a flux density function satisfying $\mathbf{f}|_{\phi=\phi_{\max}} = 0$ (possibly by cutting one of the common approaches at $\phi_{\max}$) and, for the monodisperse case, $f'(\phi_{\max}) > 0$, as postulated by Kynch.

In this work, we also employ a modification of (8), namely the formula

$$V^{\mathrm{BLS}}(\phi) := \left[\left(1 - \frac{\phi}{\phi_{\max}}\right)^n + \lambda\phi\left(\phi_{\max} - \phi\right)\right] \tag{16}$$

with parameters $n \geq 1$ and $\lambda > 0$ used by Barton *et al.* [35].

With the necessary terminology available now, we shall briefly describe the abovementioned kinematic shock tracking method, as suggested, for example, by Greenspan and Ungarish [27]. If $\mathbf{\Phi}^+$ and $\mathbf{\Phi}^-$ denote the concentrations above and below a discontinuity in the concentration field ϕ_{ij}, then its propagation speed is given by the Rankine-Hugoniot condition

$$\sigma_{ij}\left(\mathbf{\Phi}^-, \mathbf{\Phi}^+\right) = \frac{f_{ij}\left(\mathbf{\Phi}^+\right) - f_{ij}\left(\mathbf{\Phi}^-\right)}{\phi_{ij}^+ - \phi_{ij}^-}. \tag{17}$$

Assume, for example, that $\mathbf{\Phi}^+$ is known. Then (17) yields $N \cdot M$ scalar nonlinear equations for the determination of the $N \cdot M$ components of $\mathbf{\Phi}^-$ and the velocity σ_{ij}. One additonal scalar side condition will then make the computation of these quantities possible.

Consider now the settling of an initially homogeneous polydisperse suspension of K different heavy particle species at initial concentrations $\phi_1^0, \dots, \phi_K^0$. Assume that K downwards propagating kinematic shocks emerging from $z = L$ at $t = 0$ with areas of constant concentrations between each other separate the suspension at initial concentrations from the clear liquid. Then the concentrations between these shocks and the propagation velocities represent K^2 unknowns, which can be calculated from the K corresponding Rankine-Hugoniot conditions. Moreover, we assume that sediment of maximal concentration starts to form immediately at the bottom of the vessel, and that one shock line separates the sediment from the suspension at initial concentrations. It is then again possible to calculate the propagation speed plus the K concentration values below the rising discontinuity, since the sediment saturation condition $\phi_1 + \dots + \phi_K = \phi_{\max}$ provides the required scalar side condition.

This construction is valid until the fastest of the K downwards propagating kinematic shocks meets the rising one. It is assumed that these shocks join to form two new ones: a horizontal shock below which the sediment composition remains the same as before and above which a new composition of sediment satsifying the condition $\phi_1 + \dots + \phi_K = \phi_{\max}$ starts to form; and the interface between suspension and this new sediment. Above this interface, corresponding to the lowest constant concentrations section within the downwards propagating family of K shocks, the concentrations are given, so that the Rankine-Hugoniot conditions and the saturation condition provide again enough equations to calculate the new propagation speed and the sediment composition. This construction is again valid until the second fastest downwards propagating shock meets the rising sediment level, and has to be performed in total K times.

Of course, this construction presupposes that the solution of interest consists only of shock waves. In general, however, the correct solution of (13) would consist of both shock and rarefaction (smooth) waves. It is well known that there is a mathematical difficulty related to the possible non-uniqueness of solutions of conservation laws. In the theory of conservation laws, this problem is resolved by imposing additional conditions, known as entropy conditions, in order to single out the unique physically relevant solution. In particular, this means that some of the shocks used in the kinematic shock construction may be entropy violating.

A mathematically complete proof of this statement requires a detailed study of the behavior of eigenvalues and eigenvectors of the functional matrix of the system (13) and is not within the scope of this article but being prepared in [30]. However, Figures 14 and 15 in this paper seem to indicate that the first rising kinematic shock constructed by Greenspan and Ungarish [27] is not physically correct.

The problem of non-uniqueness is not of purely theoretical interest. It is also directly related to the numerical solution of systems of conservation laws such as (13). In particular, one should always employ numerical schemes which obey a discrete version of the entropy conditon. This will ensure that the scheme approximates the physically correct solution.

3. Special cases

We shall write out the system of equations (13) for the two simplest cases contained within the class of problems studied here: for the settling of initially homogeneous suspensions with two different particle sizes which are of the same density and with one particle size but different densities, respectively. Obviously, one index to denote the concentration of each species is sufficient. In the first case, we obtain

$$\frac{\partial}{\partial t}\begin{pmatrix}\phi_1\\ \phi_2\end{pmatrix} + \mu(\varrho_{\mathrm{s}}-\varrho_{\mathrm{f}})\frac{\partial}{\partial z}\left(V(\phi)(1-\phi_1-\phi_2)\begin{pmatrix}\delta_2\phi_1\phi_2-\phi_1(1-\phi_1)\\ \phi_1\phi_2-\delta_2\phi_2(1-\phi_2)\end{pmatrix}\right)=0.$$

The scalar flux density functions f_1 and f_2 involved here are plotted in [22]. In the second case, we have

$$\frac{\partial}{\partial t}\begin{pmatrix}\phi_1\\ \phi_2\end{pmatrix} + \mu\frac{\partial}{\partial z}\left(V(\phi)\begin{pmatrix}(\phi_1^3+\phi_1(1-\phi_1))\,\varrho_1+(\phi_1^2\phi_2-\phi_1)\,\varrho_2+(1-\phi_1-\phi_2)\,\varrho_{\mathrm{f}}\\ (\phi_1\phi_2^2-\phi_2)\,\varrho_1+(\phi_2^3+\phi_2(1-\phi_2))\,\varrho_2+(1-\phi_1-\phi_2)\varrho_{\mathrm{f}}\end{pmatrix}\right)=0.$$

4. Numerical scheme

The last three decades have seen a tremendous progress in the development of shock-capturing schemes for nonlinear systems of conservation laws. The term shock-capturing refers to schemes that will produce accurate approximations to discontinuous solutions without explicitly using jump conditions and shock tracking techniques. A concise introduction to these schemes is given by the book [24]. In this paper, we use the second order shock-capturing scheme developed by Nessyahu and Tadmor [31]. We briefly outline this scheme as applied to the system (13).

To approximate the solution $\mathbf{\Phi}$, we introduce a staggered mesh in the (z,t)-plane where the spatial grid points are denoted by z_j and the time levels by t_n. We denote the length of the space and time steps by Δz and Δt, respectively, i.e.,

$$\begin{aligned} z_j &= j\Delta z, \qquad j = 0, \frac{1}{2}, 1, \dots, \mathcal{J}-1, \mathcal{J}-\frac{1}{2}, \mathcal{J},\\ t_n &= n\Delta t, \qquad n = 0, \dots, \mathcal{N}, \end{aligned}$$

where $\mathcal{J}$ and $\mathcal{N}$ are integers chosen such that $\mathcal{J}\Delta z = L$ and $\mathcal{N}\Delta t = T$. For simplicity, we assume that the components of $\mathbf{\Phi}$ are arranged as a vector of K elements, i.e. $\mathbf{\Phi} = (\phi_1, \dots, \phi_K)^{\mathrm{T}}$, and that likewise $\mathbf{f}(\mathbf{\Phi}) = (f_1(\mathbf{\Phi}), \dots, f_K(\mathbf{\Phi}))^{\mathrm{T}}$.

We divide the description of the scheme into an interior part and a boundary part. We start with the interior part, which provides updating formulas for $j = \frac{1}{2}, 1, \frac{3}{2}, \dots, \mathcal{J} - \frac{3}{2}$.

4.1. **Interior scheme.** The interior scheme consists of a first order predictor step followed by a second order corrector step:

Predictor step

$$\mathbf{W}_j^{n+1/2} = \bar{\mathbf{W}}_j^n - \frac{\Delta t}{2\Delta z}\mathbf{f}_j'. \tag{18}$$

Corrector step

$$\bar{\mathbf{W}}_{j+1/2}^{n+1} = \frac{1}{2}\big(\bar{\mathbf{W}}_j^n + \bar{\mathbf{W}}_{j+1}^n\big) + \frac{1}{8}\big(\mathbf{W}_j' - \mathbf{W}_{j+1}'\big) - \frac{\Delta t}{\Delta z}\Big[\mathbf{f}\big(\mathbf{W}_{j+1}^{n+1/2}\big) - \mathbf{f}\big(\mathbf{W}_j^{n+1/2}\big)\Big], \tag{19}$$

where the vector of numerical derivatives $\mathbf{W}_j' = (w_{j,1}', \dots, w_{j,K}')^{\mathrm{T}}$ is defined by

$$w_{j,\ell}' = \mathrm{MM}\Big(2\big[\bar{w}_{j,\ell}^n - \bar{w}_{j-1,\ell}^n\big], \frac{1}{2}\big[\bar{w}_{j+1,\ell}^n - \bar{w}_{j-1,\ell}^n\big], 2\big[\bar{w}_{j+1,\ell}^n - \bar{w}_{j,\ell}^n\big]\Big), \quad \ell = 1, \dots, K, \tag{20}$$

and similarly the vector $\mathbf{f}_j' = (f_{j,1}', \dots, f_{j,K}')^{\mathrm{T}}$ is defined by

$$f_{j,\ell}' = \mathrm{MM}\Big(2\big[f_\ell(\bar{\mathbf{W}}_j^n) - f_\ell(\bar{\mathbf{W}}_{j-1}^n)\big], \frac{1}{2}\big[f_\ell(\bar{\mathbf{W}}_{j+1}^n) - f_\ell(\bar{\mathbf{W}}_{j-1}^n)\big], 2\big[f_\ell(\bar{\mathbf{W}}_{j+1}^n) - f_\ell(\bar{\mathbf{W}}_j^n)\big]\Big). \tag{21}$$

In (20) and (21), $\mathrm{MM}(a, b, c)$ is the minmod function which equals $\min(a, b, c)$ if $a, b, c > 0$, $\max(a, b, c)$ if $a, b, c < 0$, and zero otherwise. The interior scheme (18), (19) alternates between two staggered grids. In our implementation, we always start from $\bar{\mathbf{W}}_{1/2}^0$, $\bar{\mathbf{W}}_{3/2}^0, \dots, \bar{\mathbf{W}}_{\mathcal{J}-1/2}^0$, and seek to compute the values $\bar{\mathbf{W}}_1^1, \dots, \bar{\mathbf{W}}_{\mathcal{J}-1}^1$ associated with the odd time level t_1. Then, given the computed values at time level t_1, we compute the values $\bar{\mathbf{W}}_{1/2}^2, \bar{\mathbf{W}}_{3/2}^2, \dots, \bar{\mathbf{W}}_{\mathcal{J}-1/2}^2$ associated with the even time level t_2. The remaining time levels $t_3, t_4, \dots, t_N$ are treated analogously. A brief derivation of the updating formulas (18) and (19) is given in the appendix.

4.2. **Boundary scheme.** We next detail the boundary scheme that complements the interior scheme (18), (19). To this end, we write the interior scheme as

$$\bar{\mathbf{W}}_{j+1/2}^{n+1} = \frac{1}{2}\big(\bar{\mathbf{W}}_j^n + \bar{\mathbf{W}}_{j+1}^n\big) - \frac{\Delta t}{\Delta z}\Big[\mathcal{F}_{j+1} - \mathcal{F}_j\Big], \quad \mathcal{F}_j = \mathbf{f}\big(\mathbf{W}_j^{n+1/2}\big) + \frac{1}{8}\frac{\Delta z}{\Delta t}\mathbf{W}_j'. \tag{22}$$

Roughly speaking, the boundary treatment consists in setting the numerical fluxes $\mathcal{F}_j$ to zero at the lower and upper boundaries according to the boundary conditions (15). However, since the interior scheme is based on a staggered grid, the boundary treatment consists of two alternating steps, which take the following respective forms:

i) n even: We are given the values $\bar{\mathbf{W}}^n_{1/2}, \bar{\mathbf{W}}^n_{3/2}, \dots, \bar{\mathbf{W}}^n_{\mathcal{J}-1/2}$, and seek to compute the odd time level values $\bar{\mathbf{W}}^{n+1}_{1/4}, \bar{\mathbf{W}}^{n+1}_{1}, \dots, \bar{\mathbf{W}}^{n+1}_{\mathcal{J}-1}, \bar{\mathbf{W}}^{n+1}_{\mathcal{J}-1/4}$. On the lower boundary, we use

$$\bar{\mathbf{W}}^{n+1}_{1/4} = \bar{\mathbf{W}}^n_{1/2} - 2\frac{\Delta t}{\Delta z}\mathcal{F}_{1/2}, \quad \bar{\mathbf{W}}^n_{-1/2} := \bar{\mathbf{W}}^n_{1/2}, \tag{23}$$

where the auxiliary value $\bar{\mathbf{W}}^n_{-1/2}$ is used in computing the numerical flux $\mathcal{F}_{1/2}$. In other words, we use one-sided differences to calculate the numerical derivatives at $z = z_{1/2}$. On the upper boundary, we use

$$\bar{\mathbf{W}}^{n+1}_{\mathcal{J}-1/4} = \bar{\mathbf{W}}^n_{\mathcal{J}-1/2} + 2\frac{\Delta t}{\Delta z}\mathcal{F}_{\mathcal{J}-1/2}, \quad \bar{\mathbf{W}}^n_{\mathcal{J}+1/2} := \bar{\mathbf{W}}^n_{\mathcal{J}-1/2}, \tag{24}$$

where the auxiliary value $\bar{\mathbf{W}}^n_{\mathcal{J}+1/2}$ is used in computing $\mathcal{F}_{\mathcal{J}-1/2}$. In particular, this means that we use one-sided differences when computing numerical derivatives at $z = z_{\mathcal{J}-1/2}$.

ii) n odd: We are given the values $\bar{\mathbf{W}}^n_{1/4}, \bar{\mathbf{W}}^n_{1}, \dots, \bar{\mathbf{W}}^n_{\mathcal{J}-1}, \bar{\mathbf{W}}^n_{\mathcal{J}-1/4}$, and seek to compute the values $\bar{\mathbf{W}}^{n+1}_{1/2}, \bar{\mathbf{W}}^{n+1}_{3/2}, \dots, \bar{\mathbf{W}}^{n+1}_{\mathcal{J}-1/2}$. On the lower boundary, we use

$$\bar{\mathbf{W}}^{n+1}_{1/2} = \frac{1}{2}\big(\bar{\mathbf{W}}^n_0 + \bar{\mathbf{W}}^n_1\big) - \frac{\Delta t}{\Delta z}\mathcal{F}_1, \quad \bar{\mathbf{W}}^n_0 := \bar{\mathbf{W}}^n_{1/4}, \tag{25}$$

where the extrapolated value $\bar{\mathbf{W}}^n_0$ is used also in computing the numerical flux $\mathcal{F}_1$. On the upper boundary, we use

$$\bar{\mathbf{W}}^{n+1}_{\mathcal{J}-1/2} = \frac{1}{2}\big(\bar{\mathbf{W}}^n_{\mathcal{J}-1} + \bar{\mathbf{W}}^n_{\mathcal{J}}\big) + \frac{\Delta t}{\Delta z}\mathcal{F}_{\mathcal{J}-1}, \quad \bar{\mathbf{W}}^n_{\mathcal{J}} := \bar{\mathbf{W}}^n_{\mathcal{J}-1/4}, \tag{26}$$

where the extrapolated value $\bar{\mathbf{W}}^n_{\mathcal{J}}$ is used also in computing the numerical flux $\mathcal{F}_{\mathcal{J}-1}$. A brief derivation of the updating formulas (23)–(26) is given in the appendix.

It is a well accepted practice to utilize conservative methods when solving numerically systems of conservation laws [24]. Shock waves are the solution features which require this treatment. It is well known that if a conservative method converges, it does so to a weak solution of the conservation law. Moreover, if the scheme also satisfies a discrete entropy principle, the converged solution is the physical weak solution. We emphasize that the second order predictor-corrector scheme of Nessyahu and Tadmor [31] is conservative and that it also satisfies a discrete entropy principle and thus produces physically correct solutions.

5. Numerical simulations

In the following, we first present numerical simulations of published experimental data of the settling of polydisperse suspensions, and then simulate sedimentation of polydisperse suspensions in some hypothetical configurations exhibiting interesting settling behaviour. The spatial discretization parameter used was $\Delta z = L/800$; the time step was chosen by

$$\Delta t = 0.45\Delta z / \max_{i,j} |r_{\infty ij}|, \tag{27}$$

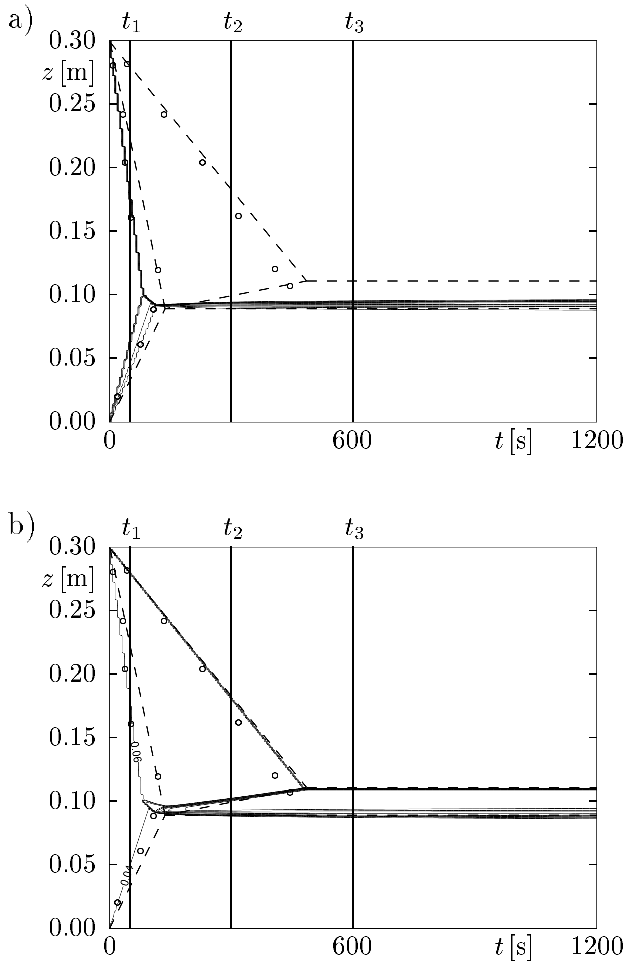

FIGURE 1. Settling of a bidisperse suspension of heavy particles of two different sizes: iso-concentration lines (a) of the larger particles and (b) of the smaller particles, corresponding to the values of ϕ_i 0.02, 0.04, 0.06, 0.08, 0.1, 0.15, 0.25, 0.3, 0.4, 0.5 and 0.6. The circles and the dashed lines correspond to experimental measurements of interface locations and shock lines, respectively, obtained by Schneider *et al.* [26]. Concentration profiles taken at the times t_1, t_2 and t_3 are given in Figure 3.

where $r_{\infty ij}$ is given by (11). The coefficient 0.45 yields a slight underestimate of the maximally admissible time step for the staggered grid given by replacing 0.45 in (27) by 0.5.

5.1. **Comparison with published results.**

5.1.1. *Settling of a bidisperse suspension.* Consider the experiment performed by Schneider, Anestis and Schaflinger [26] with glass beads of the same density $\varrho_{\mathrm{s}} = 2790\,[\mathrm{kg/m^3}]$ and of the diameters $d_1 = 0.496\,[\mathrm{mm}]$ and $d_2 = 0.125\,[\mathrm{mm}]$ in a settling column of height $L =$

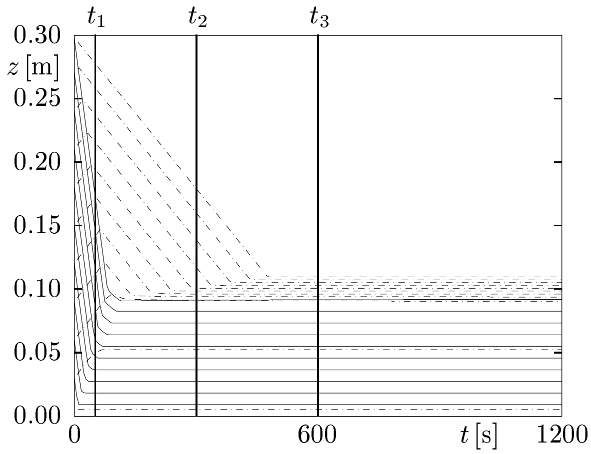

FIGURE 2. Settling of a bidisperse suspension of heavy particles of two different sizes: particle trajectories of the larger particles (solid lines) and of the smaller particles (dashdotted lines). Concentration profiles taken at the times t_1, t_2 and t_3 are given in Figure 3.

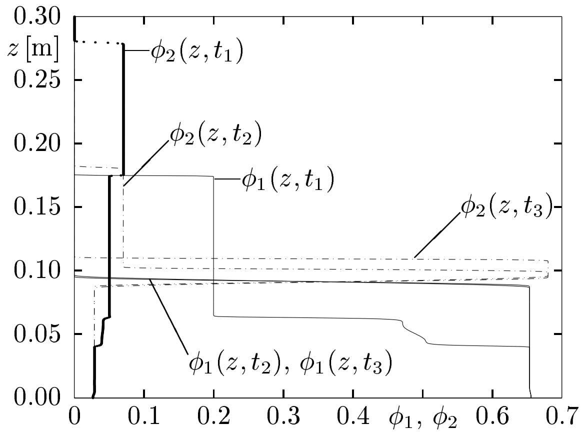

FIGURE 3. Settling of a bidisperse suspension of heavy particles of two different sizes: concentration profiles of the larger particles (index 1) and of the smaller particles (index 2) at $t_1 = 51.9$ [s], $t_2 = 299.8$ [s] and $t_3 = 599.7$ [s].

0.3 [m]. The fluid density and viscosity are $\varrho_{\mathrm{f}} = 1208\,[\mathrm{kg/m^3}]$ and $\mu_{\mathrm{f}} = 0.02416\,[\mathrm{kg\,m^{-1}s^{-1}}]$, respectively. The initial concentrations are $\phi_1^0 = 0.2$ and $\phi_2^0 = 0.05$, and the simulated time here is $T = 1200$ [s]. Following Schneider *et al.* [26], we employ Richardson and Zaki's flux density function given in (8) with $n = 2.7$, which is cut at $\phi_{\max} = 0.68$, see Concha *et al.* [22]. Figure 1 displays the simulated iso-concentration lines for each species, together with the experimental measurements of interface locations and computed shock lines made by Schneider and coauthors, while Figure 3 shows concentration profiles of both species at three selected times.

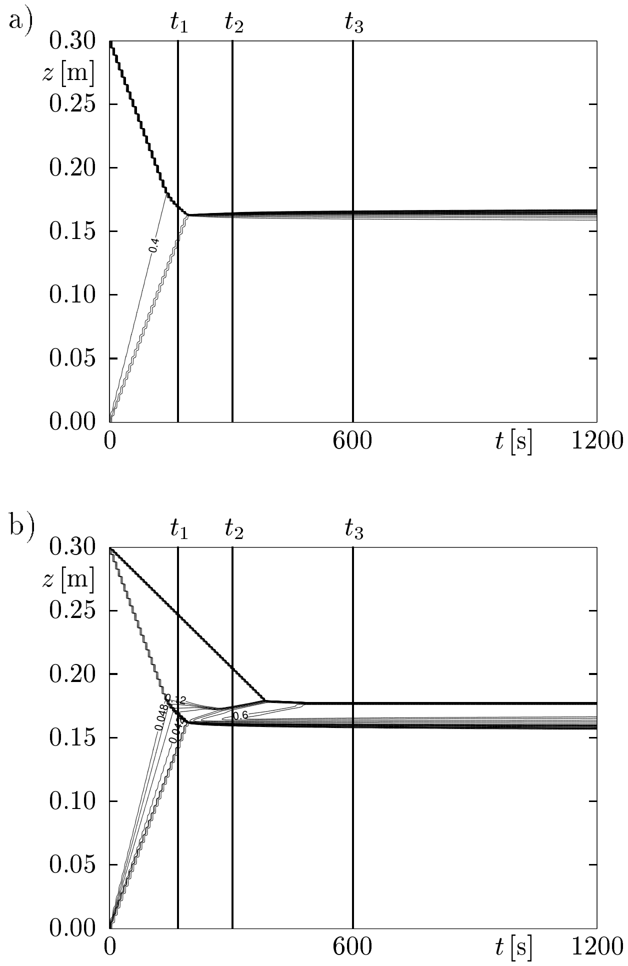

FIGURE 4. Settling of a bidisperse suspension of heavy particles of two different sizes: iso-concentration lines (a) of the larger particles and (b) of the smaller particles, corresponding to the values of ϕ_i 0.02, 0.032, 0.038, 0.04, 0.042, 0.044, 0.046, 0.048, 0.06, 0.08, 0.1, 0.12, 0.14, 0.16, 0.18, 0.2, 0.25, 0.3, 0.4, 0.5, 0.6 and 0.65. Concentration profiles taken at the times t_1, t_2 and t_3 are given in Figure 5. In Figure 6, the upper left quarter of the settling plot for the smaller particles is shown together with relevant parts of numerical results from [22].

Following Gaudin and Fuerstenau [36] and Tiller *et al.* [37], we construct 'Lagrangian paths' to follow given sets of particles of each species. Integrating the concentration data at a given time with respect to height yields the heights under which 1%, 10%, 20%, ..., 90 and 99% of the total mass of the particle species are located. The succession of these points with respect to time yields curves which may be considered as trajectories of particles initially separated by 1% from the remaining 99% (and so on) of total mass of that species. With the exception of the 1% line of the heavy particles, the particle trajectories

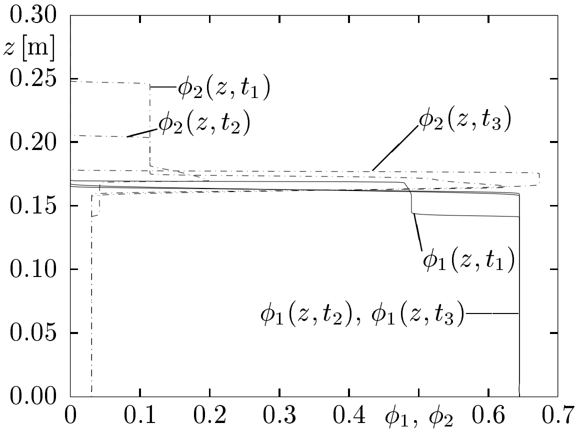

FIGURE 5. Settling of a bidisperse suspension of heavy particles of two different sizes: concentration profiles of the larger particles (index 1) and of the smaller particles (index 2) at $t_1 = 168.2\,[\mathrm{s}]$, $t_2 = 302.7\,[\mathrm{s}]$ and $t_3 = 598.7\,[\mathrm{s}]$.

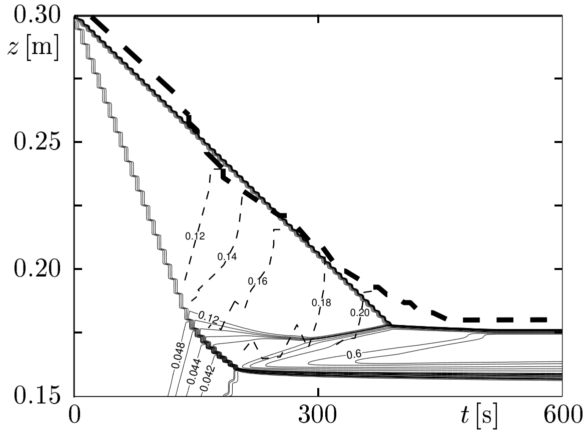

FIGURE 6. Detail of Figure 4 (b). In addition, some iso-concentration lines for the smaller particles computed by Concha *et al.* [22] are shown.

computed from the concentration data of Figure 1 are shown in Figure 2. Figure 1 shows a good agreement of simulated and experimental results and Figure 2 shows clearly that the small particles have initially an upward constant movement before settling at constant rate as if they were alone in the suspension.

In addition to the original initial data used by Schneider *et al.* [26], Concha *et al.* [22] considered also a hypothetical settling experiment of the same bidisperse suspension with the considerably increased initial concentrations $\phi_1^0 = 0.35$ and $\phi_2^0 = 0.05$. The simulated time is again $T = 1200\,[\mathrm{s}]$. The numerical results are shown in Fig. 4 and 5. Figure 6 shows that our numerical results for this problem differ in some regions significantly from the results in [22], which were computed by a finite difference algorithm due to Lee [38].

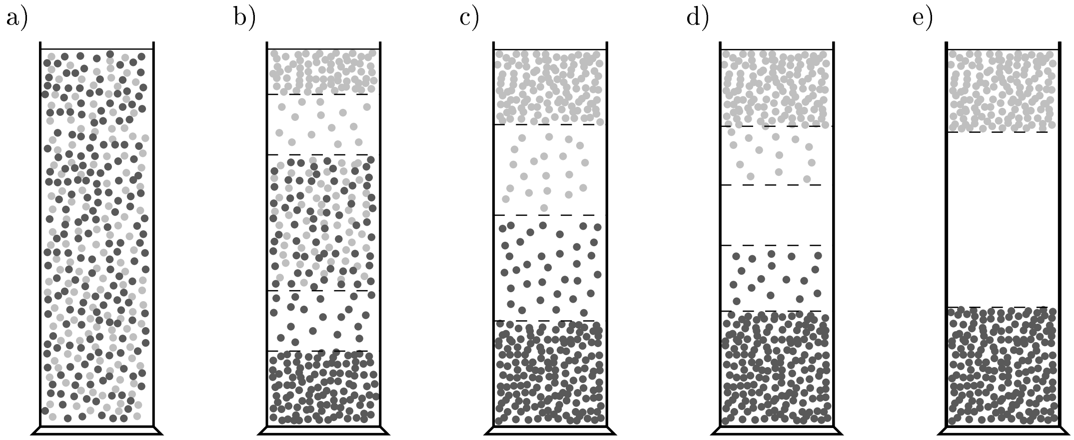

FIGURE 7. Different stages during separation of a suspension of heavy (dark) and light (bright) particles, see also [23, Fig. 8]: (a) initial state of the suspension, (b) streaming period, (c) point of separation into monodisperse suspensions, (d) settling of the two species as monodisperse suspensions, (e) fully settled sediments.

In particular, we believe that the strange behaviour of the interface between clear liquid and suspension, marked by the fat dashed line in Figure 6, might be due to an error in Lee's rather complicated interface tracking algorithm [38].

5.1.2. *Separation of a bisdisperse suspension with light and heavy particles.* Fessas and Weiland [39, 40] and Weiland and MacPherson [41] study the increase of settling rates of a given monodisperse suspension of heavy particles if lighter, buoyant particles are added. This phenomenon has been studied by Law *et al.* [21] as a comparison example for several of the mathematical models for polydisperse suspensions reviewed in the introduction in combination with experimental measurements. To demonstrate the effect of the presence of both light and heavy particles, we select one of the configurations considered by Law *et al.* [21]: the solid particles are of the same size and of the densities $\varrho_2 = 1050\,[\mathrm{kg/m^3}]$ and $\varrho_1 = 1186\,[\mathrm{kg/m^3}]$, while the fluid density and viscosity are $\varrho_{\mathrm{f}} = 1120\,[\mathrm{kg/m^3}]$ and $\mu_{\mathrm{f}} = 0.000141\,[\mathrm{kg\,m^{-1}s^{-1}}]$, respectively. Figure 7 illustrates schematically the stages observed during the separation process.

The experimental sedimentation container used by Law *et al.* was rather narrow such that wall effects could not be neglected. Thus the final settling velocities resulting from insertion of these parameters into the Stokes formula (11) were corrected (reduced in modulus by roughly 10%), leading to $r_{\infty 1} = -0.001241\,[\mathrm{m/s}]$ and $r_{\infty 2} = 0.001348\,[\mathrm{m/s}]$. Furthermore, the authors state that the exponent $n = 5.39$, of the Richardson-Zaki approach, fitted settling data of monodisperse suspensions of each of the particle species best. The Richardson-Zaki flux density function was cut now at $\phi_{\max} = 0.6713$. In the experiment simulated here, the suspension was of initial height $0.283\,[\mathrm{m}]$ and contained initially 8% of each solid species.

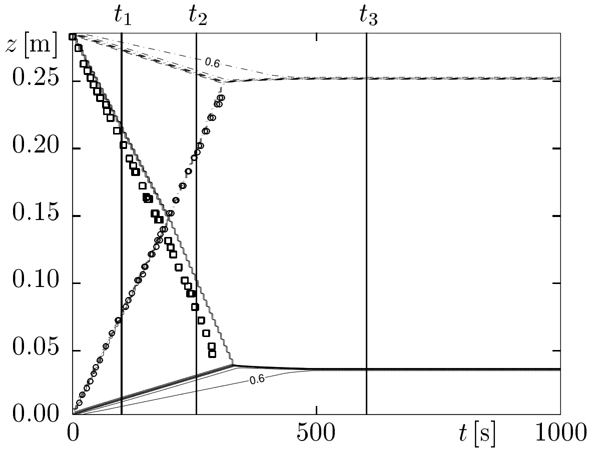

FIGURE 8. Settling of a bidisperse suspension of heavy and light (buoyant) particles: iso-concentration lines of the heavy particles (solid lines) and of the light particles (dashdotted), corresponding to the values 0.025, 0.05, 0.075, 0.1, 0.2, 0.3, 0.4, 0.5 and 0.6. The squares and circles correspond to experimental measurements of the settling curves of the light and of the heavy particles, repectively, performed by Law *et al.* [21]. Concentration profiles taken at the times t_1, t_2 and t_3 are given in Figure 10.

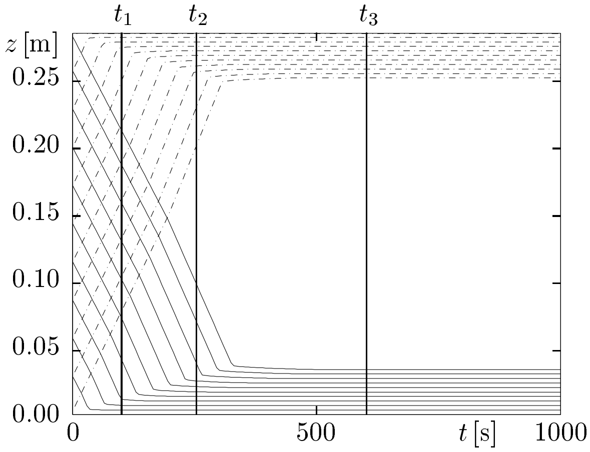

FIGURE 9. Settling of a bidisperse suspension of heavy and light (buoyant) particles: particle trajectories of the heavy (solid lines) and of the light particles (dashdotted lines). Concentration profiles taken at the times t_1, t_2 and t_3 are given in Figure 10.

In [21], only the intersecting interface curves of both species are displayed for $t \lesssim 320\,[\mathrm{s}]$; here the complete separation process is shown for $t \leq T = 1000\,[\mathrm{s}]$. Figure 10 shows concentration profiles for both species at three selected times, Figure 8 shows the iso-concentration lines for both species (the qualitatively different behavior of both species

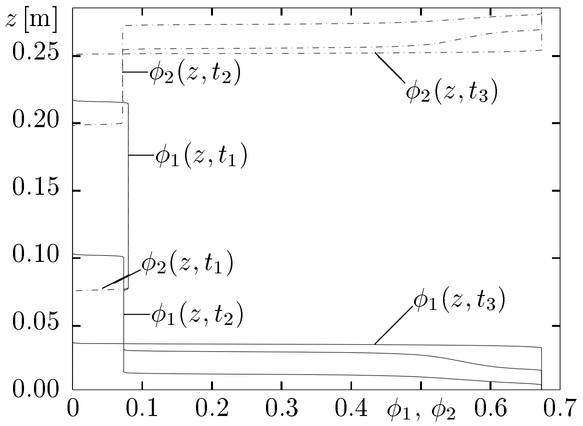

FIGURE 10. Settling of a bidisperse suspension of heavy and light (buoyant) particles: concentration profiles of the larger particles (index 1) and of the smaller particles (index 2) at $t_1 = 100.4$ [s], $t_2 = 253.9$ [s] and $t_3 = 602.3$ [s].

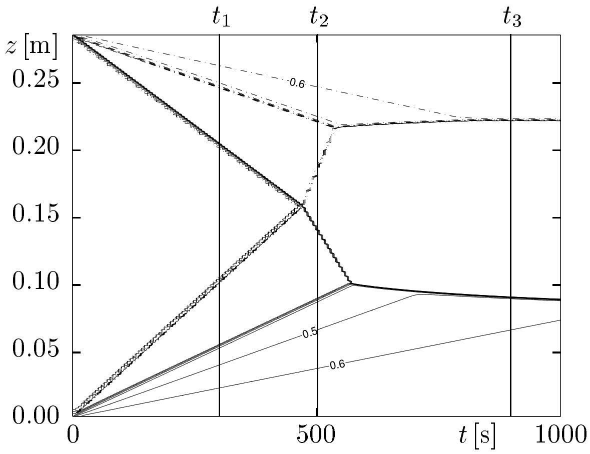

FIGURE 11. Settling of a bidisperse suspension of heavy and light (buoyant) particles: iso-concentration lines of the heavy particles (solid lines) and of the light particles (dashdotted), corresponding to the values 0.025, 0.05, 0.075, 0.1, 0.15, 0.2, 0.3, 0.4, 0.5 and 0.6. Concentration profiles taken at the times t_1, t_2 and t_3 are given in Figure 13.

makes it possible to collect the respective settling plots into one diagram), and Figure 9 presents the particle trajectories which were obtained in the same way as in the previous example.

The results illustrate that the numerical scheme predicts correctly the expected separation behaviour. Figure 8 indicates that both phases are already entirely separated at $t = t_2$, and that the final state of the suspension consists of two sediments of maximum solids concentration separated by clear liquid.

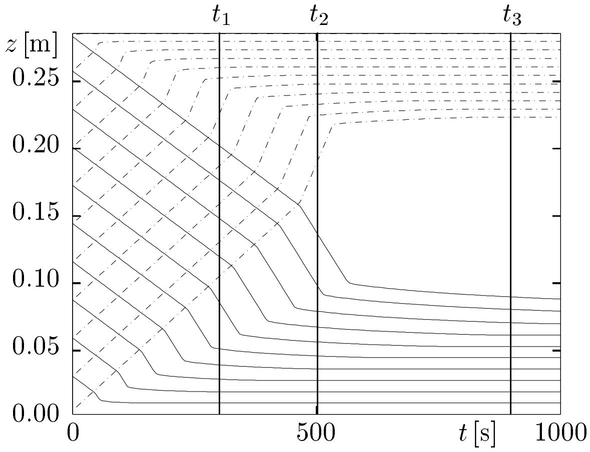

FIGURE 12. Settling of a bidisperse suspension of heavy and light (buoyant) particles: particle trajectories of the heavy (solid lines) and of the light particles (dashdotted lines). Concentration profiles taken at the times t_1, t_2 and t_3 are given in Figure 13.

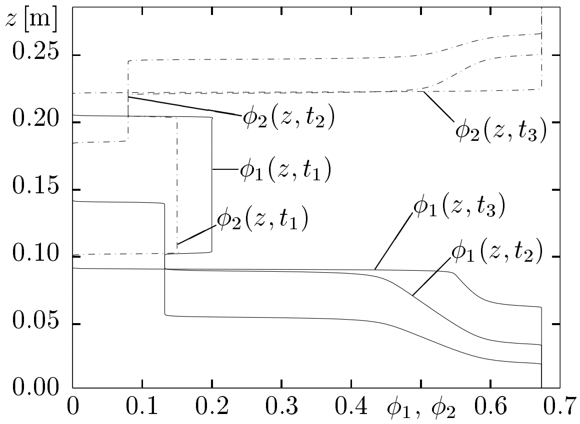

FIGURE 13. Settling of a bidisperse suspension of heavy and light (buoyant) particles: concentration profiles of the larger particles (index 1) and of the smaller particles (index 2) at $t_1 = 301.1$ [s], $t_2 = 501.9$ [s] and $t_3 = 897.5$ [s].

We also simulate a second experiment perfomed by Law *et al.* [21]; namely, we take $\phi_1^0 = 0.20$ and $\phi_2^0 = 0.15$ and leave the remaining parameters unchanged. The corresponding numerical results are given in Figures 11, 12 and 13. By the behaviour of the iso-concentration lines corresponding to $\phi_1 = 0.5$, $\phi_1 = 0.6$ and $\phi_2 = 0.6$ and by the shapes of the 'edges' of the sediment layers forming at the top and at the bottom of the column, respectively, these results make the occurrence of rarefaction waves apparent. Moreover, Figure 13 shows that at $t = t_3$, by its sharp edge, the upper sediment is already in its final state, in contrast to the lower.

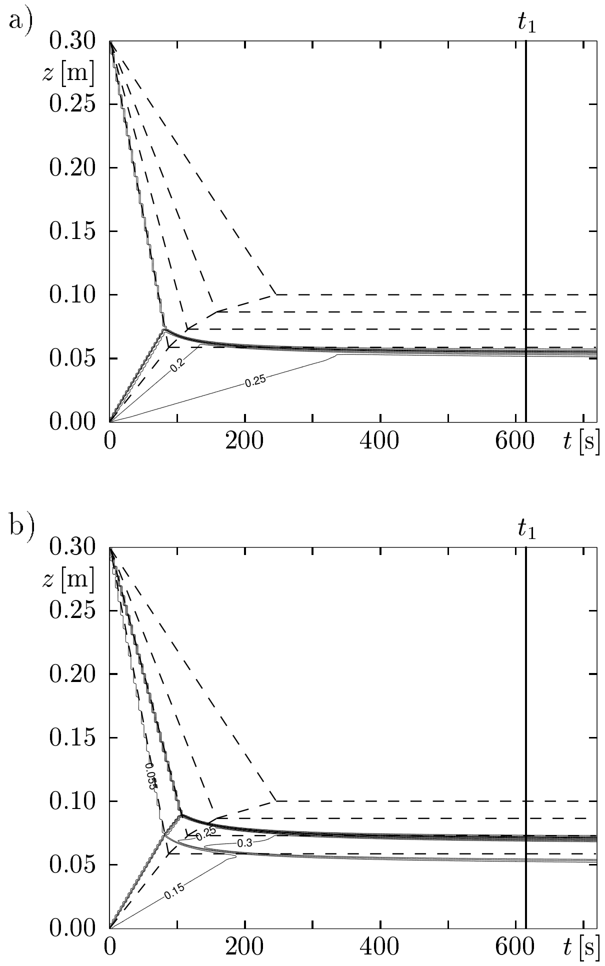

FIGURE 14. Settling of a suspension of heavy particles of four different sizes: iso-concentration lines of a) the largest, b) the second largest particles, corresponding to the values 0.005, 0.03, 0.055, 0.08, 0.1, 0.15, 0.2, 0.25, 0.3, 0.4, 0.5 and 0.6. The dashed lines correspond to kinematic shock lines calculated by Greenspan and Ungarish [27]. The concentration profiles at time t_1 are included in Fig. 16.

It should be mentioned that our numerical results differ substantially from the behaviour of this suspension observed by Law *et al.* [21]: their photograph clearly illustrates that at high initial concentrations in a suspension with buoyant particles, lateral segregation between heavy and light solids during separation occurs. Macroscopically, this movement becomes visible as an intrinsically two-dimensional 'fingering' effect (see [42]) and is therefore out of the scope of the one-dimensional model considered here. This conclusion had also been drawn by Shih *et al.* [23] who simulated a similar experiment by a one-dimensional hydrodynamical model including compression effects.

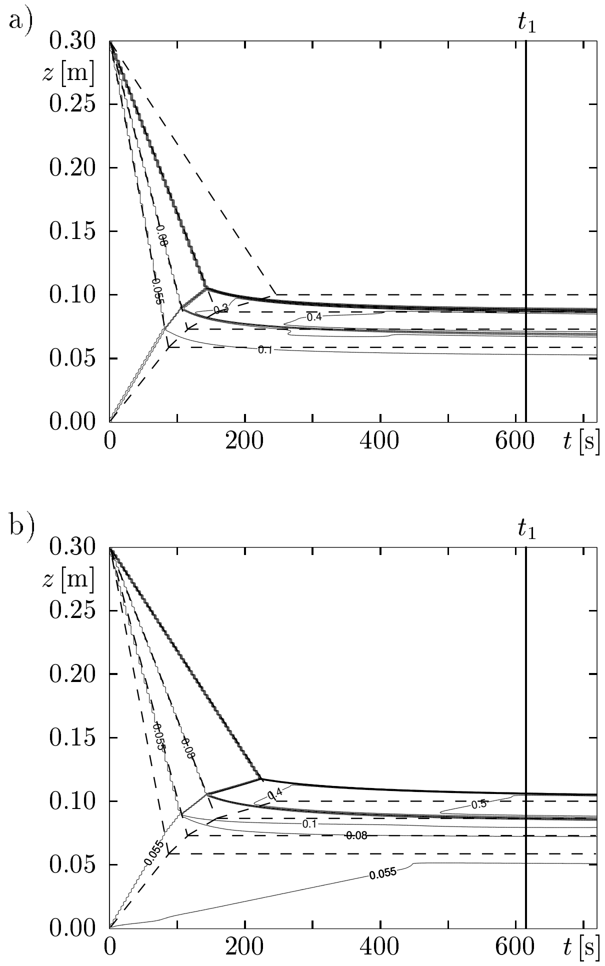

FIGURE 15. Settling of a suspension of heavy particles of four different sizes: iso-concentration lines of a) the second smallest, b) the smallest particles, corresponding to the values 0.005, 0.03, 0.055, 0.08, 0.1, 0.15, 0.2, 0.25, 0.3, 0.4, 0.5 and 0.6. The dashed lines correspond to kinematic shock lines calculated by Greenspan and Ungarish [27]. The concentration profiles at time t_1 are included in Fig. 16.

5.1.3. *Sedimentation of a suspension with particles of four different sizes.* In [27], Greenspan and Ungarish consider the settling of a polydisperse suspension of four different sizes. They use the function (in our notation)

$$V(\phi) = V^{\mathrm{GU}}(\phi) := \left(1 - \frac{\phi}{\phi_{\max}}\right)^2, \quad \phi_{\max} = 0.6 \tag{28}$$

and represent their solution in dimensionless variables. To make their result comparable with the previous calculations, we select, as in the first example, $\varrho_{\mathrm{s}} = 2790\,[\mathrm{kg/m^3}]$, $\varrho_{\mathrm{f}} = 1208\,[\mathrm{kg/m^3}]$, $\mu_{\mathrm{f}} = 0.02416\,[\mathrm{kg\,m^{-1}s^{-1}}]$, $L = 0.3\,[\mathrm{m}]$ and $d_1 = 0.496\,[\mathrm{mm}]$. The smaller

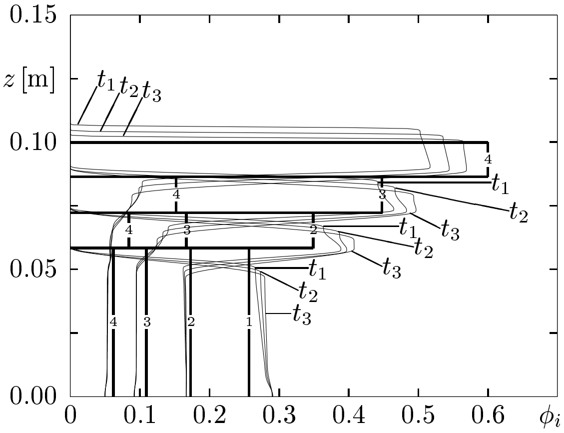

FIGURE 16. Settling of a suspension of heavy particles of four different sizes: concentration profiles of species 1 to 4 at $t_1 = 615.07\,[\mathrm{s}]$, $t_2 = 999.5\,[\mathrm{s}]$ and $t_3 = 2000.0\,[\mathrm{s}]$. The horizontal and vertical lines are the stationary kinematic shock solution (the number i corresponds to species i, $i = 1, \dots, 4$) by Greenspan and Ungarish [27]. The approximation of their solution indicates which numerically calculated concentration profile calculated here belongs to which species.

particles are assumed to be of the diameters $d_2 = 0.8d_1 = 0.3968\,[\mathrm{mm}]$, $d_3 = 0.6d_1 = 0.2976\,[\mathrm{mm}]$ and $d_4 = 0.4d_1 = 0.1984\,[\mathrm{mm}]$. The constant initial concentrations are $\phi_1^0 = \phi_2^0 = \phi_3^0 = \phi_4^0 = 0.05$. In Figures 14 and 15, we show the solution represented by iso-concentration lines for $t \leq T = 720\,[\mathrm{s}]$. The particle trajectories turned out very similar to those of Figure 2 and are therefore not depicted.

Greenspan and Ungarish [27] determine a solution of the same problem within the class of picecewise constant functions, separated by kinematic shocks as outlined above. To make comparison possible, their solution is also drawn in Figures 14 and 15. Their result implies, in particular, that the sediment composition remains constant for all times once the discontinuity separating the suspension in hindered settling from the clear liquid has reached the sediment level. Our numerical solution for large times is compared with their result in Figure 16.

This example illustrates that the scheme is able to treat systems of more than two particle species. Figures 14 and 15 suggest, by the incidence with the shock lines computed by our numerical methods, that the kinematic shock construction is in this case correct for the family of shock lines emerging from $(z,t) = (L,0)$. However, the construction of a single shock emerging from $(z,t) = (0,0)$ appears no to be correct, and is replaced here by a rarefaction wave, which starts to interact earlier with the fastest downwards traveling shock, see Figure 14 (a). Although the transient settling process simulated numerically is quite different from the kinematic shock construction, the results for the sediment composition given in Figure 16 for large times are comparable. However, note that the behaviour of the profiles of ϕ_3 and ϕ_4 below the respective zones where these concentrations are dominant suggest that continuous transitions also have to be considered as part of steady state solutions.

5.2. **Hypothetical test cases.**

5.2.1. *Rarefaction waves in a bidisperse suspension.* The preceding examples illustrate what is well known from the theory of monodisperse ideal suspensions: sediment is not only composed by kinematic shocks and their interactions; rather than that, the effect of rarefaction waves has to be taken into account. We present now two examples imposing initial conditions which, in view of comparable results known from the sedimentation behaviour of monodisperse suspensions, can be expected to produce rarefaction waves.

In the first case, consider a 'membrane problem': we assume that the upper half of the settling column is initially filled with a bidisperse suspension, while its lower half contains pure liquid:

$$\phi_1^0(z) = \phi_2^0(z) = \begin{cases} 0.1 & \text{for } z \geq 0.15\,[\mathrm{m}], \\ 0 & \text{for } z < 0.15\,[\mathrm{m}]. \end{cases}$$

The remaining parameters are identical to the data used by Schneider *et al.* [26]. The simulated time is $T = 900\,[\mathrm{s}]$. The results are given in Figures 17 and 18. Note that the spreading of the trajectories of the smaller particles visible in Figure 18 corresponds to the formation of a rarefacation wave.

In the second example, we illustrate the effect obtained if the initial concentration distribution is chosen such that the larger particles will 'overtake' the smaller ones:

$$\phi_1^0(z) = \begin{cases} 0.1 & \text{for } z \geq 0.225\,[\mathrm{m}], \\ 0 & \text{for } z < 0.225\,[\mathrm{m}], \end{cases} \quad \phi_2^0(z) = \begin{cases} 0.1 & \text{for } 0.15\,[\mathrm{m}] \leq z < 0.225\,[\mathrm{m}], \\ 0 & \text{otherwise.} \end{cases}$$

Note that now the initial state consists of a piecewise monodisperse suspension. Figure 19 shows the corresponding particle trajectories for a simulated time $T = 250\,[\mathrm{s}]$. The iso-concentration lines look very similar to the previous example and are therefore omitted. It can be seen in Figure 19 that the larger particles start to settle at unique and constant speed, while the smaller form a rarefaction wave. The species then interact and mutual hindrance makes the settling of both slower. The passage of the larger particles through the smaller causes also the former to form a rarefaction wave. Note that the largest particles have settled completely before the first of the smaller arrive at the top of the sediment layer.

5.2.2. *Settling of a mixed polydisperse suspension with different particle sizes and different densities.* So far, we have considered only mixtures in which the particle species differ either in size or in density. However, the model equations permit that particles differ in both properties. To demonstrate the effects occurring in such a system, we chose an example of four different particle species ($N = M = 2$) having the properties given in Table 1, where m_{ij} denotes the mass of species ij. The relevant properties of the fluid are again $\varrho_{\mathrm{f}} = 1208\,[\mathrm{kg/m^3}]$ and $\mu_{\mathrm{f}} = 0.02416\,[\mathrm{kg\,m^{-1}s^{-1}}]$.

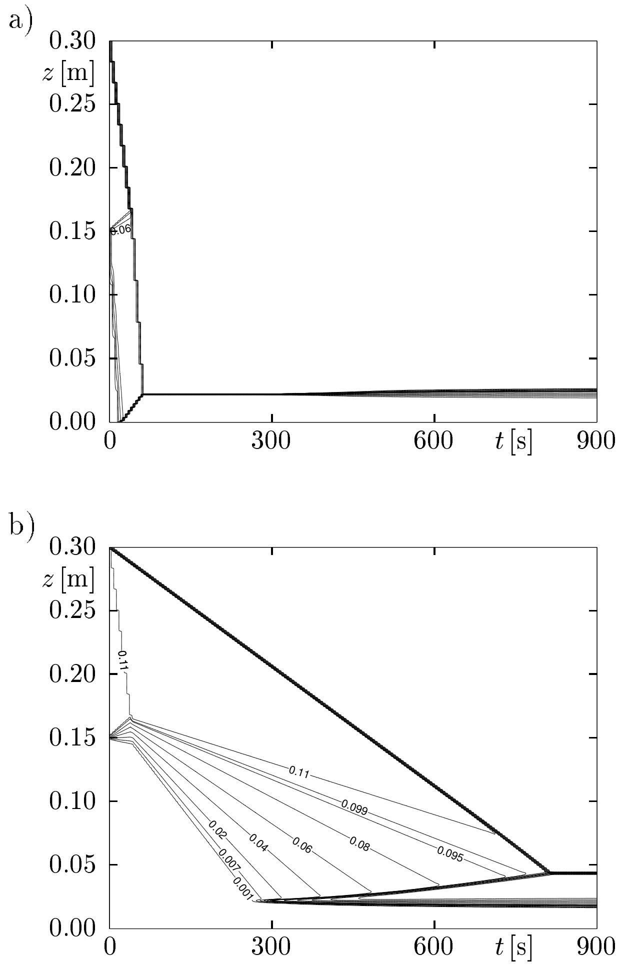

FIGURE 17. Settling of a bidisperse suspension of heavy particles of two different sizes initially located above clear liquid: iso-concentration lines (a) of the larger particles and (b) of the smaller particles, corresponding to the values of ϕ_i 0.001, 0.007, 0.02, 0.04, 0.06, 0.08, 0.095, 0.099, 0.11, 0.20, 0.3, 0.4, 0.5 and 0.6.

The parameters have been selected such that all four species have different particle mass while the second and third heaviest species possess equal final settling velocity. A classical experiment with one pair of particle species differing in size and density but having the same final settling velocity was conducted by Richardson and Meikle [43], see also [19, 44]. In this case, we employed the drag law (16) proposed by Barton *et al.* [35], whose parameters $\phi_{\max} = 0.6$, $n = 5$ and $\lambda = 5/59$ have been adopted. The Kynch flux density function corresponding to this choice possesses two inflection points and satisfies $f'(\phi_{\max}) > 0$. Consequently, any rarefaction wave emerging from $z = 0$, $t = 0$ will be finite, i.e. not contain characteristics of infinitely small slope, in contrast to what happens if the Richardson-Zaki drag law is used without cutting it at a maximum concentration

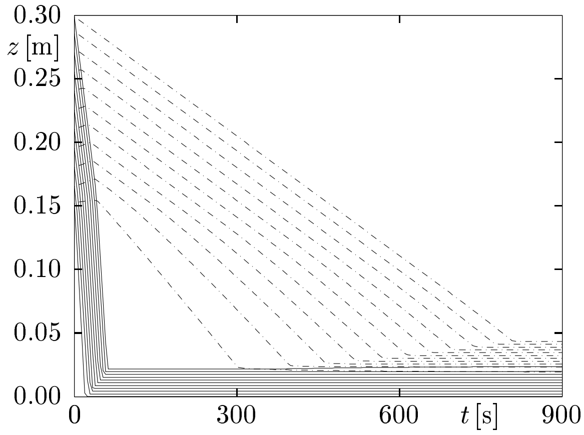

FIGURE 18. Settling of a bidisperse suspension of heavy particles of two different sizes initially located above clear liquid: particle trajectories of the heavy (solid lines) and of the light particles (dashdotted lines).

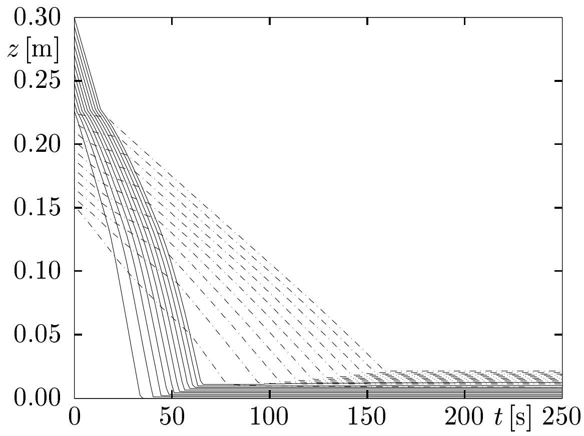

FIGURE 19. Settling of a bidisperse suspension of heavy particles of two different sizes with picewise monodisperse initial states: particle trajectories of the larger particles (solid lines) and of the smaller particles (dashdotted lines).

$\phi_{\max} < 1$. This means that the batch sedimentation process should terminate after finite time.

The numerical solution of this example is depicted in Figures 20, 21 and 22. Calculations were performed for a simulated time of $T = 4000\,[\mathrm{s}]$. Indeed, all iso-concentration lines become horizontal. Unfortunately, severe diffusion somewhat distorts the results. This becomes evident by the spreading of closeby iso-concentration lines, which are meant to denote a kinematic shock of the exact solution.

i	j	d_i [mm]	ϱ_j [kg/m^3]	m_{ij} [10^{-3}g]	$r_{\infty ij}$ [10^{-3} m/s]
1	1	0.5	2790.00	0.1826	-8.922
1	2	0.5	2220.48	0.1453	-5.710
2	1	0.4	2790.00	0.0935	-5.710
2	2	0.4	2220.48	0.0744	-3.654

TABLE 1. Properties of the particles of the mixed polydisperse suspension

The main reason for this undesirable effect is the coexistence of physical phenomena within the sedimentation model which propagate both at very small and at large velocities. That is, some of the concentrations quickly tend to develop stationary or almost stationary shocks, while this takes much longer time for others. With explicit schemes as the one employed here, however, the time step is limited by the fastest moving concentration component. Consequently, explicit schemes limit the time step to a much smaller value than is actually sufficient to accurately resolve the transient behaviour of the slowly moving components. For the particular scheme used here, this becomes apparent by the excessive diffusion in the concentration isolines corresponding to the lightest or smallest particle species when performing long time integration. A detailed study of this phenomenon produced by the numerical scheme and possible strategies for its correction are presented in [30].

6. Conclusions

We have shown that the use of modern shock capturing schemes represents a serious alternative to the shock tracking techniques that have been proposed for the simulation of settling of polydisperse suspensions. This is illustrated by the agreement with experimental data and the fact that there are no principal problems in treating large numbers of particle species. Moreover, these schemes obey an entropy principle and therefore approximate the unique physically relevant solution. This becomes apparent by several test cases in which the scheme replaces a constructed kinematic shock by a rarefaction wave.

The scheme used in this paper is a high-resolution scheme which is particularly easy to implement. For completeness, the (few) necessary formulas for implementing the scheme have been included in this paper. It is also possible to consider other schemes. A comparative study of some modern shock-capturing schemes for simulating the settling of polydispersed suspensions is presented in [30].

We suggest employing these schemes for the study of several additional problems that could not be considered here, for example for the study of fluidization problems such as bed inversion [45], for the testing of Davis and Gecol's new parameterless hindered settling function [33], as these authors suggest, for tridisperse and more complex suspensions, and for the simulation of the transient behaviour of polydisperse suspensions in mineral processing applications such as density separation [46]. On the other hand, the severe

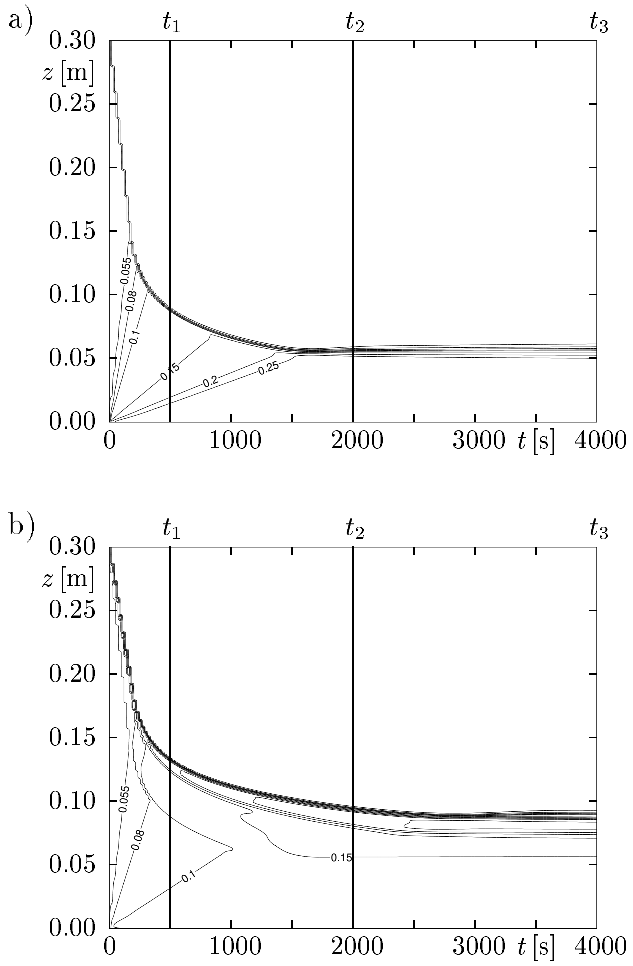

FIGURE 20. Settling of a suspension of heavy particles of two different sizes and two different densities: iso-concentration lines of a) the heaviest, b) the second heaviest particles, corresponding to the values of ϕ_{ij} 0.005, 0.03, 0.055, 0.08, 0.1, 0.15, 0.2, 0.25, 0.3, 0.4, 0.5 and 0.6. The concentration profiles at times t_1, t_2 and $t_3 = T$ are given in Fig. 22.

limitations of kinematic sedimentation models have become evident for monodisperse suspensions, since most industrial slurries develop compressible sediments which a kinematic theory cannot describe. Therefore the rigorous phenomenological model developed for monodisperse flocculated suspensions [47] should be extended to polydisperse mixtures, following, for example, Stamatakis and Tien [48]. Also for such models it should be possible to apply shock-capturing schemes, following, e.g., the splitting approach implemented in the monodisperse case by Bustos *et al.* [5].

7. List of symbols

d_i	diameter of particle species ij

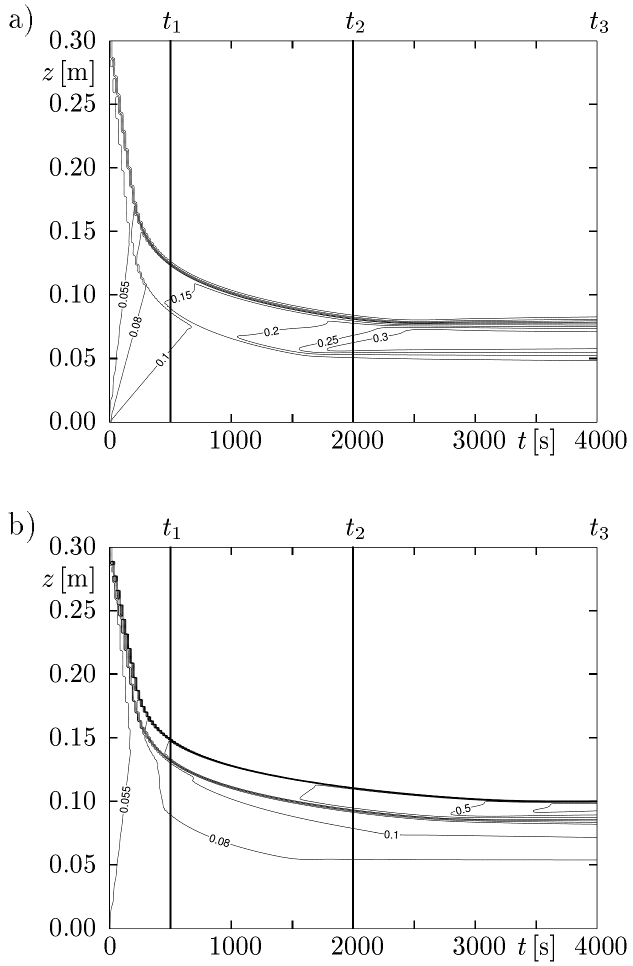

FIGURE 21. Settling of a suspension of heavy particles of two different sizes and two different densities: iso-concentration lines of a) the second lightest, b) the lightest particles, corresponding to the values of ϕ_{ij} 0.005, 0.03, 0.055, 0.08, 0.1, 0.15, 0.2, 0.25, 0.3, 0.4, 0.5 and 0.6. The concentration profiles at times t_1, t_2 and $t_3 = T$ are given in Fig. 22.

$f(\phi)$	Kynch batch flux density function
$f_{ij}(\mathbf{\Phi})$	flux density function for particle species ij
$\mathbf{f}$	flux density vector
$\mathbf{f}'_j$	approximate derivative used by numerical scheme
$\mathfrak{F}_j$	numerical flux
g	acceleration of gravity
j	space step index used by numerical scheme
$\mathfrak{J}$	number of space intervals
K	assumed number of particle species
L	height of the settling column

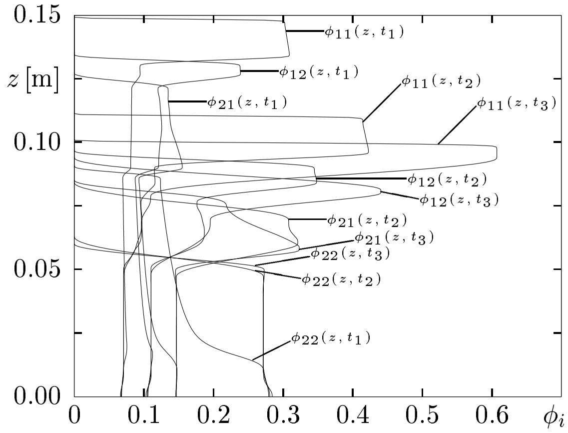

FIGURE 22. Settling of a suspension of heavy particles of two different sizes and two different densities: concentration profiles of each species at $t_1 = 499.3\,[\mathrm{s}]$, $t_2 = 1997.4\,[\mathrm{s}]$ and $t_3 = T = 4000$.

M	number of different particle densities
$\mathrm{MM}(\cdot,\cdot,\cdot)$	minmod function used by numerical scheme
n	exponent in drag law formulas
n	time step index used by numerical scheme
N	number of different particle diameters
$\mathcal{N}$	number of time intervals
q	volume average velocity
r_{ij}	relative velocity between particle species ij and the fluid
$r_{\infty ij}$	Stokes settling velocity of a single particle of species ij
t	time
t_n	discrete time
T	endpoint of simulated time interval
v_{f}	local velocity of the fluid
v_{ij}	phase velocity of particle species ij
v_{s}	solids phase velocity
$V(\phi)$	drag law or hindered settling function
$\mathbf{W}(z,t_n)$	numerical approximation
$\bar{\mathbf{W}}_j^n$	cell average used by numerical scheme
$\bar{\mathbf{W}}^{n+1}_{-1/2,1/4,\mathcal{J}-1/4,\mathcal{J}+1/2}$	auxiliary values used by the boundary scheme
$\mathbf{W}_j^{n+1/2}$	predictor value used by numerical scheme
$\bar{\mathbf{W}}_{j+1/2}^{n+1}$	corrector value used by numerical scheme
$\mathbf{W}_j'$	approximate derivative used by numerical scheme
z	height
z_j	discrete height

Greek letters.

δ_i	ratio d_i^2/d_1^2
Δt, Δz	discretization parameters
λ	parameter in Barton, Li and Spencer's formula
μ	a parameter in the definition of f_{ij}
μ_{f}	viscosity of the fluid
ϕ	solids total volume fraction
ϕ_0	homogeneous initial concentration of a monodisperse suspension
$\phi_0(z)$	initial concentration distribution of a monodisperse suspension
ϕ_{ij}	volumetric concentration of particle species ij
$\phi_{ij}^0(z)$	initial distribution of ϕ_{ij}
$\phi_{\max}$	maximum concentration
$\mathbf{\Phi}$	matrix of concentration values ϕ_{ij}
ϱ_{f}	fluid density
ϱ_j	density of particle species ij
ϱ_{s}	solids density
σ_{ij}	jump propagation velocity

Acknowledgements

KKF and KHK are grateful to the group of Prof. Dr.-Ing. W.L. Wendland at the Institute of Mathematics A, University of Stuttgart, for hospitality. The preparation of this paper was made possible by travel grants awarded by the European Science Foundation (ESF) through the Applied Mathematics in Industrial Flow Problems (AMIF) programme. Support by the Sonderforschungsbereich 404 at the University of Stuttgart is also gratefully acknowledged. We also acknowledge support of Fondef project D97-I2042.

References

[1] R. Aris and N.R. Amundson, Mathematical Methods in Chemical Engineering, Vol.2: First-Order Partial Differential Equations with Applications, Prentice-Hall, Englewood Cliffs, NJ, USA, 1973.

[2] M.C. Bustos and F. Concha, 'Kynch theory of sedimentation', Chapter 2 in E. Tory (ed.), Sedimentation of Small Particles in a Viscous Fluid, Computational Mechanics Publications, Southampton, UK, 1996, 7–49.

[3] G.J. Kynch, 'A theory of sedimentation', Trans. Farad. Soc. 48 (1952), 166–176.

[4] M.C. Bustos and F. Concha, 'On the construction of global weak solutions in the Kynch theory of sedimentation', Math. Meth. Appl. Sci. 10 (1988), 245–264.

[5] M.C. Bustos, F. Concha, R. Bürger and E.M. Tory, Sedimentation and Thickening: Phenomenological Foundation and Mathematical Theory, to be published by Kluwer Academic Publishers, Dordrecht, The Netherlands, 1999.

[6] M.C. Bustos, F. Concha and W.L. Wendland, 'Global weak solutions to the problem of continuous sedimentation of an ideal Suspension', Math. Meth. Appl. Sci. 13 (1990), 1–22.

[7] S. Diehl, 'A conservation law with point source and discontinuous flux function modelling continuous sedimentation', SIAM J. Math. Appl. 56 (1996), 388–419.

[8] S. Diehl, 'Dynamic and steady-state behaviour of continuous sedimentation', SIAM J. Appl. Math. 57 (1997), 991–1018.

[9] S. Diehl, 'Continuous sedimentation of multi-component particles', Math. Meth. Appl. Sci. 20 (1997), 1345–1364.
[10] C.A. Petty, 'Continuous sedimentation of a suspension with nonconvex flux law', Chem. Engrg. Sci. 30 (1975), 1451–1458.
[11] R. Bürger, W.L. Wendland and F. Concha, 'Model equations for gravitational sedimentation-consolidation processes', submitted to Z. Angew. Math. Mech.
[12] R. Bürger, M.C. Bustos and F. Concha, 'Settling velocities of particulate systems: 9. Phenomenological theory of sedimentation processes: Numerical simulation of the transient behaviour of flocculated suspensions in an ideal batch or continuous thickener', Int. J. Mineral Process. 55 (1999), 267–282.
[13] R. Bürger and F. Concha, 'Mathematical model and numerical simulation of the settling of flocculated suspensions', Int. J. Multiphase Flow 24 (1998), 1005–1023.
[14] T.N. Smith, 'The differential sedimentation of particles of two different sizes', Trans. Instn. Chem. Engrs. 43 (1965), T69–T73.
[15] T.N. Smith, 'The sedimentation of particles having a dispersion of sizes', Trans. Instn. Chem. Engrs. 44 (1966), T152–T157.
[16] M.J. Lockett and H.M. Al-Habbooby, 'Differential settling by size of two particles in a liquid', Trans. Instn. Chem. Engrs. 51 (1973), 281–292.
[17] M.J. Lockett and H.M. Al-Habbooby, 'Relative particle velocities in two-species settling', Powder Technol. 10 (1974), 67–71.
[18] S. Mirza and J.F. Richardson, 'Sedimentation of suspensions of particles of two or more sizes', Chem. Engrg. Sci. 34 (1979), 447–454.
[19] J.H. Masliyah, 'Hindered settling in a multiple-species particle system', Chem. Engrg. Sci. 34 (1979), 1166–1168.
[20] V.S. Patwardhan and C. Tien, 'Sedimentation and liquid fluidization of solid particles of differenz sizes and densities', Chem. Engrg. Sci. 40 (1985), 1051–1060.
[21] H.S. Law, J.H. Masliyah, R.S. MacTaggart and K. Nandakumar, 'Gravity separation of bisdisperse suspensions: light and heavy particle species', Chem. Engrg. Sci. 42 (1987), 1527–1538.
[22] F. Concha, C.H. Lee and L.G. Austin, 'Settling velocities of particulate systems: 8. Batch sedimentation of polydispersed suspensions of spheres', Int. J. Mineral Process. 35 (1992), 159–175.
[23] Y.T. Shih, D. Gidaspow and D.T. Wasan, 'Hydrodynamics of sedimentation of multisized particles', Powder Technol. 50 (1987), 201–215.
[24] R.J. Le Veque, Numerical Methods for Conservation Laws, Second Ed., Birkhäuser Verlag, Basel 1992.
[25] A. Kluwick, 'Kinematische Wellen', Acta Mechanica 26 (1977), 15–46.
[26] W. Schneider, G. Anestis and U. Schaflinger, 'Sediment composition due to settling of particles of different sizes', Int. J. Multiphase Flow 11 (1985), 419–423.
[27] H.P. Greenspan and M. Ungarish, 'On hindered settling of particles of different sizes', Int. J. Multiphase Flow 8 (1982), 587–604.
[28] M.S. Selim, A.C. Kothari and R.M. Turian, 'Sedimentation of multisized particles in concentrated suspensions',
[29] K. Stamatakis and C. Tien, 'Dynamics of batch sedimentation of polydispersed suspensions', Powder Technol. 56 (1988), 105–117.
[30] R. Bürger, K.-K. Fjelde and K.H. Karlsen, 'Numerical methods for systems of conservation laws modelling sedimentation of polydisperse suspensions', in preparation.
[31] H. Nessyahu and E. Tadmor, 'Non-oscillatory central differencing for hyperbolic conservation laws', J. Comp. Phys. 87 (1990), 408–463.
[32] J.F. Richardson and W.N. Zaki, 'Sedimentation and fluidization I', Trans. Inst. Chem. Eng. (London) 32 (1954), 35–53.
[33] R.H. Davis and H. Gecol, 'Hindered settling function with no empirical parameters for polydisperse suspensions', AIChE J. 40 (1994), 570–575.

[34] G.B. Wallis, One-dimensional Two-phase Flow, McGraw-Hill Book Co., New York 1969.
[35] N.G. Barton, C.H. Li and S.J. Spencer, 'Control of a surface of discontinuity in continuous thickeners', J. Austral. Math. Soc. Ser. B 33 (1992), 269–280.
[36] A.M. Gaudin and M.C. Fuerstenau, 'Experimental and mathematical model of thickening', Trans. AIME 223 (1962), 122–129.
[37] F.M. Tiller, N.B. Hsyung and Y.L. Shen, 'CATSCAN analysis of sedimentation and constant pressure filtration', Proc. of the V World Filtration Congress, Société Française de Filtration, Nice, France 1991, vol.2, 80–85.
[38] C.H. Lee, *Modeling of Batch Hindered Settling*, PhD thesis, College of Earth and Mineral Sciences, Pennsylvania State University, University Park, PA, USA, 1989.
[39] Y.P. Fessas and R.H. Weiland, 'Convective solids settling induced by a buoyant phase', AIChE J. 27 (1981), 588–592.
[40] Y.P. Fessas and R.H. Weiland, 'The settling of suspensions promoted by rigid buoyant particles', Int. J. Multiphase Flow 10 (1984), 485–507.
[41] R.H. Weiland and R.R. McPherson, 'Accelerated settling by addition of buoyant particles', Ind. Engrg. Chem. Fund. 18 (1979), 45–49.
[42] R.H. Weiland, Y.P. Fessas and B.V. Ramarao, 'On instabilities arising during sedimentation of two-component mixtures of solids', J. Fluid Mech. 142 (1984), 383–389.
[43] J.F. Richardson and R.A. Meikle, 'Sedimentation and fluidization. Part III: The sedimentation of uniform fine particles and of two-component mixtures of solids. Trans. Inst. Chem. Engrs. 39 (1961), 348–356.
[44] J.M. Coulson, J.F. Richardson, J.R. Backhurst and J.H. Harker, Chemical Engineering. Vo. 2, Fourth Edition: Particle Technology and Separation Processes, Butterworth-Heinemann, Oxford, UK, 1991.
[45] N. Epstein and B.P. Le Clair, 'Liquid fluidization of binary particle mixtures—II. Bed inversion', Chem. Engrg. Sci. 40 (1985), 1517–1526.
[46] Y. Zimmels, 'Theory of density separation of particulate systems', Powder Technol. 43 (1985), 127–139.
[47] F. Concha, M.C. Bustos and A. Barrientos, 'Phenomenological theory of sedimentation', Ch. 3 in E. Tory (ed.), Sedimentation of Small Particles in a Viscous Fluid, Computational Mechanics Publications, Southampton, UK, 1996, 51–96.
[48] K. Stamatakis and C. Tien, 'Batch sedimentation calculations—the effect of compressible sediment', Powder Technol. 72 (1992), 227–240.
[49] D. Levy and E. Tadmor, 'Non-oscillatory boundary treatment for staggered central schemes', UCLA-CAM Report 1, 1998.

Appendix. Brief derivation of the numerical scheme

In this appendix we briefly derive the difference formulas introduced in §4. As mentinoned in §4, we divide the description of the scheme into an interior part, i.e., formulas (18) and (19), and a boundary part, i.e., formulas (23) to (26).

7.1. **Interior scheme.** At time level t_n, given the cell averages $\{\bar{\mathbf{W}}_j^n\}_j$ (see below), we introduce a piecewise linear approximate solution $\mathbf{W}(z,t_n) \approx \mathbf{\Phi}(z,t_n)$ of the form

$$\mathbf{W}(z,t_n) = \bar{\mathbf{W}}_j^n + \frac{1}{\Delta z}\mathbf{W}_j'(z - z_j) \quad \text{for } z \in \left[z_{j-1/2}, z_{j+1/2}\right], \tag{29}$$

where $\mathbf{W}_j' = (w_{j,1}', \dots, w_{j,K}')^{\mathrm{T}}$ is the slope vector defined in (20). In particular, this choice of slope vector satisfies (see [31])

$$\frac{1}{\Delta z}\mathbf{W}_j' = \frac{\partial}{\partial z}\mathbf{W}(z = z_j, t_n) + \mathcal{O}(\Delta z),$$

which ensures second order accuracy wherever the components of $\boldsymbol{\Phi}$ are smooth. In addition, this choice ensures that the approximation is non-oscillatory. We refer to [31] for other choices of slope vectors. Now integrating the conservation laws

$$\frac{\partial}{\partial t}\mathbf{W} + \frac{\partial}{\partial z}\mathbf{f}(\mathbf{W}) = 0 \tag{30}$$

over $[z_j, z_{j+1}] \times [t_n, t_{n+1}]$ yields the following exact evolution equation of $\mathbf{W}$:

$$\bar{\mathbf{W}}_{j+1/2}^{n+1} = \bar{\mathbf{W}}_{j+1/2}^{n} - \frac{1}{\Delta z}\left[\int_{t_n}^{t_{n+1}} \mathbf{f}(\mathbf{W}(z_{j+1}, t))\, dt - \int_{t_n}^{t_{n+1}} \mathbf{f}(\mathbf{W}(z_{j-1}, t))\, dt\right], \tag{31}$$

where $\bar{\mathbf{W}}_{j+1/2}^{n}$ is the cell average defined by

$$\bar{\mathbf{W}}_{j+1/2}^{n} = \frac{1}{\Delta z}\int_{z_j}^{z_{j+1}} \mathbf{W}(z, t_n)\, dz, \tag{32}$$

and similarly for $\bar{\mathbf{W}}_{j+1/2}^{n+1}$. Note that explicit expressions for the integral averages given by (32) can be deduced easily from (29). In fact,

$$\bar{\mathbf{W}}_{j+1/2}^{n} = \frac{1}{2}(\bar{\mathbf{W}}_j^n + \bar{\mathbf{W}}_{j+1}^n) + \frac{1}{8}(\bar{\mathbf{W}}_j' - \bar{\mathbf{W}}_{j+1}').$$

For a sufficiently small time step Δt, the time integrals in (31) only involve smooth integrands (due to the staggering) so that they can be computed within any degree of accuracy by an appropriate quadrature rule, see [31]. Here, the time integrals of the flux are approximated by the second order accurate mid-point rule,

$$\frac{1}{\Delta z}\int_{t_n}^{t_{n+1}} \mathbf{f}(\mathbf{W}(z_j, t))\, dt \approx \frac{\Delta t}{\Delta z}\mathbf{f}(\mathbf{W}(z_j, t_{n+1/2})),$$

where the point-values at the half time steps are evaluated by Taylor expansion,

$$\mathbf{W}_j^{n+1/2} := \mathbf{W}(z_j, t_{n+1/2}) \approx \mathbf{W}(z_j, t_n) + \frac{\Delta t}{2}\frac{\partial}{\partial t}\mathbf{W}(z_j, t = t_n) = \bar{\mathbf{W}}_j^n - \frac{\Delta t}{2\Delta z}\mathbf{f}_j'. \tag{33}$$

Here, the slope vector $\mathbf{f}_j' = (f_{j,1}', \dots, f_{j,K}')^{\mathrm{T}}$ is defined in (21). In particular, this choice of slope vector ensures second order accuracy in smooth regions, i.e.,

$$\frac{1}{\Delta z}\mathbf{f}_j' = \frac{\partial}{\partial z}\mathbf{f}(\mathbf{W}(z = z_j, t_n)) + \mathcal{O}(\Delta z),$$

and that the numerical approximation is non-oscillatory, see [31]. Summing up, we end up with the interior scheme (18)-(19). We refer to Nessyahu and Tadmor [31] for further details on the derivation of the interior scheme.

7.2. **Boundary scheme.** We next derive the formulas (23)–(26), i.e., the boundary scheme. Let us first derive (23), where the auxiliary value $\bar{\mathbf{W}}_{1/4}^{n+1}$ denote the average of $W(z, t_{n+1})$ on the boundary half-cell $[z_0, z_{1/2}]$ centered around $z_{1/4}$,

$$\bar{\mathbf{W}}_{1/4}^{n+1} = \frac{2}{\Delta z} \int_{z_0}^{z_{1/2}} \mathbf{W}(z, t_{n+1})\, dz.$$

The concept of boundary half-cells was introduced by Levy and Tadmor [49] in their treatment of Dirichlet boundary conditions for the Nessyahu and Tadmor scheme [31]. We emphasize that the boundary scheme used in this paper is not derived in [31, 49].

Integrating the conservation law (30) over $[z_0, z_{1/2}] \times [t_n, t_{n+1}]$ and taking into account that the physical flux should according to (15) vanish at $z = z_0$, we get

$$\bar{\mathbf{W}}_{j+1/4}^{n+1} = \bar{\mathbf{W}}_{j+1/4}^{n} - \frac{2}{\Delta z} \int_{t_n}^{t_{n+1}} \mathbf{f}(\mathbf{W}(z_{1/2}, t))\, dt. \tag{34}$$

Using (29) with $j = \frac{1}{2}$, a straightforward computation reveals that

$$\bar{\mathbf{W}}_{1/4}^{n} := \frac{2}{\Delta z} \int_{z_0}^{z_{1/2}} \mathbf{W}(z, t_n)\, dz = \bar{\mathbf{W}}_{1/2}^{n} - \frac{1}{4} \bar{\mathbf{W}}'_{1/2}.$$

Using this and the mid-point rule to replace the time integral in (34), we obtain

$$\bar{\mathbf{W}}_{1/4}^{n+1} = \bar{\mathbf{W}}_{1/2}^{n} - \frac{1}{4} \bar{\mathbf{W}}'_{1/2} - 2\frac{\Delta t}{\Delta z} \mathbf{f}(\mathbf{W}_{1/2}^{n+1/2}),$$

which is precisely (23) if we identify the predictor value $\mathbf{W}_{1/2}^{n+1/2}$ as (33) with $j = 1/2$. This predictor value becomes well-defined once we introduce the auxiliary value $\bar{\mathbf{W}}_{-1/2}^{n} := \bar{\mathbf{W}}_{1/2}^{n}$; In other words, we use one-sided differences to calculate the numerical derivatives at $z = z_{1/2}$. Defining the auxiliary values $\bar{\mathbf{W}}_{\mathcal{J}-1/4}^{n}$ and $\bar{\mathbf{W}}_{\mathcal{J}-1/4}^{n+1}$ as the averages on the boundary half-cell $[z_{\mathcal{J}-1/2}, z_{\mathcal{J}}]$ of $\mathbf{W}(z, t)$ at $t = t_n$ and $t = t_{n+1}$, respectively, the formula (24) for the upper boundary can be derived similarly.

Let us now derive (25). Using the updating formula (22) with $j = 0$, we get

$$\bar{\mathbf{W}}_{1/2}^{n+1} = \frac{1}{2}\big(\bar{\mathbf{W}}_{0}^{n} + \bar{\mathbf{W}}_{1}^{n}\big) - \frac{\Delta t}{\Delta z}\Big[\mathcal{F}_1 - \mathcal{F}_0\Big],$$

where $\bar{\mathbf{W}}_{0}^{n} := \bar{\mathbf{W}}_{1/4}^{n}$. Now (25) is obtained by simply setting $\mathcal{F}_0 := 0$. The formula (26) for the upper boundary is obtained similarly.

This concludes the discussion of the boundary scheme.